

Introducing a Method for Evaluating Fabric Performance against Human Body Thermal Radiation

Elham Tavakkol^{1*}, Abolghasem Zeidaabadi Nezhad², Sedigheh Borhani¹

¹ Department of Textile Engineering, Isfahan University of Technology, Isfahan, Iran.

² Department of Electrical and Computer Engineering, Isfahan University of Technology, Isfahan, Iran.

Article Information	Abstract
Article history: Received: 2025-05-25 Accepted: 2025-09-22	More than half of the body's metabolic heat is dissipated to the environment as infrared radiation. Consequently, the design and development of textiles that modulate infrared radiation to provide localized heating or cooling have recently gained significant attention for enhancing thermal comfort. However, evaluating the performance of such textiles often requires specialized and costly methods. This study introduces a novel approach for assessing the optical properties of fabrics in the infrared region by utilizing Fourier-transform infrared (FTIR) spectroscopy data and calculating key scattering parameters. The calculated spectra demonstrated that fabric samples incorporating 1% and 2% aluminum (designated PA1 and PA2) reflect more than 40% of human body radiation near the skin, thereby effectively inhibiting radiative heat loss to the environment. The significant apparent temperature difference observed for these samples confirmed their potential as effective radiative heating textiles. The findings indicate that the proposed method offers a viable and accessible alternative for the relative evaluation and comparison of textile thermal radiation properties, especially in settings where advanced instrumentation like an integrating sphere is unavailable.
Keywords: Woven fabric; Thermal radiation management; Infrared spectroscopy; Scattering parameters.	

1 INTRODUCTION

Approximately 40-60% of the heat generated by the human body is transferred to the surroundings via infrared (IR) rays [1]. Thus, regulating the thermal radiation properties of fabrics can greatly influence the localized warming or cooling of the human body [2]. In recent years, efforts have been made to produce textiles with unique characteristics against IR radiation of the human body [2-11]. Based on the principle of energy conservation, to minimize the heat radiation loss from the body in thermal fabrics, at least one of the following cases must be achieved: high reflectance (R) from the inner surface of the fabric, low emittance (E) from the outer surface of the fabric, and low transmittance (T) through the fabric thickness [2, 11]. The most common methods for evaluating the performance of textiles against IR involve the use of Fourier-transform infrared (FTIR) spectrometers equipped with an integrated golden sphere, artificial skin, and an IR camera [1]. In our previous studies [12, 13], we investigated the thermal, optical, and mechanical properties of fabrics made from polypropylene (PP) fibers containing aluminum (Al) particles (PP/Al). These fabrics have suitable wearable and durable properties for passive radiative heating clothing. Using numerical full-wave analysis, the optimal size and content of spherical Al microparticles were identified to minimize the heat radiation transmission through the PP/Al fabrics. Then, the thermal radiation properties of the produced fabrics were

evaluated using IR spectroscopy by measuring the IR transmittance and emittance. Additionally, the increase in skin temperature was measured using an IR thermometer [13]. Conventional FTIR spectrometers can only measure transmittance (at an angle of incidence θ_i of 0°) or reflectance (at $\theta_i = 45^\circ$) by the attenuated total reflection (ATR) method [13]. Recently, we found that by using FTIR transmittance data and ATR spectroscopy data, it is possible to calculate the attenuation coefficient (α) and refractive index (n) of the fabrics, respectively. Then, the reflectance, transmittance, and emittance spectra can be calculated at $\theta_i = 0^\circ$ in the whole studied wavelength range using the transmission (ABCD) matrix. Therefore, in this study, a novel method is proposed for calculating the attenuation coefficient, refractive index, and spectral characteristics of the reflectance (R), transmittance (T), and emittance (E) using FTIR data, without the need for advanced equipment such as an integrating sphere. This approach can serve as a practical and accessible tool for evaluating the thermal performance of textile materials, especially in situations where access to sophisticated instruments is limited.

2 MATERIALS AND METHODS

2-1 Fabric Sample Production

Four samples of woven fabric were produced using a

* Corresponding author: e.tavakkol@tx.iut.ac.ir

weaving machine (twill 3/1, Picanol OptiMax, Belgium). Commercial polyester yarn (110 denier) was selected as the warp yarn for all samples, and polypropylene yarn containing different amounts of Al (0%, 1%, and 2%) produced by the melt spinning method was used as the weft yarn for the fabric production of PP, PA1, and PA2, respectively (Table 1). The warp density was maintained constant at 57 threads/cm for all samples, and the maximum weft density was used for fabric weaving. The PET fabric sample was woven under the same conditions using a commercial polyester weft yarn [13]. The area density and thickness of the fabrics were measured based on the ASTM D3776 and ISO 1243 standards, respectively (surface of 1000 mm² under pressure of 1 kPa). Although the maximum weft density was targeted for all samples, the incorporation of Al particles altered the spinability and physical properties of the PP/Al yarns, as evidenced by the reduction in their linear density (Table 1). This, in turn, led to variations in the final achievable weft density and other fabric structural parameters. These variations are an inherent result of the Al modification, and they provide insight into the profound impact of the additive on the entire yarn and fabric system.

2-2 Optical properties of the fabrics

Fig. 1 shows the schematic of the fabric exposed to an IR laser beam in the FTIR device. A FTIR spectrometer (Bomem MB 100, Canada) was used to measure the overall IR transmittance within the 8-14 μm wavelength range, with a 4 cm^{-1} resolution. The average thickness of the fabric samples, measured based on ISO 1243 standards, is reported in Table 1. But for the FTIR spectroscopy measurements, to ensure consistency and accuracy in the optical tests, areas with a consistent thickness were identified, marked, and used on each fabric sample ($d = 260 \mu\text{m}$).

The attenuation coefficient (α) of the fabric samples with a d thickness was calculated according to their FTIR spectrum (T) and Equation (1) [14].

$$T = e^{-2\alpha d} \quad (1)$$

The specular IR reflectance from the surface of all the fabric samples was determined by the ATR method at an angle of 45°. Each fabric specimen was placed on the ZnSe crystal of the ATR accessory. Then, the spectrum measurements were conducted in the 8–14 μm wavelength range with an 8 cm^{-1} resolution. The effective refractive index (N_{eff}) of each sample [15] was calculated using the built-in software based on Kramers-Krönig integral [16]. Using the calculated

refractive index, the intrinsic impedance of the medium (η) could be obtained at each wavelength (λ) by

$$\eta = \frac{\eta_0}{N_{\text{eff}}} \quad (2)$$

Where η_0 is the intrinsic impedance of the free space. IR transmittance $T = |S_{21}|^2$ and reflectance $R = |S_{11}|^2$ were calculated using the transmission (ABCD) matrix [17]:

$$\begin{bmatrix} A & B \\ C & D \end{bmatrix} = \begin{bmatrix} \cosh\left(\frac{2\pi N_{\text{eff}} d}{\lambda} j + \alpha d\right) & \eta \sinh\left(\frac{2\pi N_{\text{eff}} d}{\lambda} j + \alpha d\right) \\ \frac{1}{\eta} \sinh\left(\frac{2\pi N_{\text{eff}} d}{\lambda} j + \alpha d\right) & \cosh\left(\frac{2\pi N_{\text{eff}} d}{\lambda} j + \alpha d\right) \end{bmatrix} \quad (3)$$

Where α , η , λ , d , and N_{eff} are described above. At each wavelength, S_{21} and S_{11} parameters were calculated using the following relations [17]:

$$S_{21} = \frac{2}{A + \frac{B}{\eta_{\text{air}}} + C\eta_{\text{air}} + D}, \quad S_{11} = \frac{A + \frac{B}{\eta_{\text{air}}} - C\eta_{\text{air}} - D}{D} \quad (4)$$

The detector in the FTIR mode cannot determine the IR reflectance. Meanwhile, after the IR beam incident on the surface, the principle of energy conservation is satisfied:

$$T + R + A = 1 \quad (5)$$

Where the absorbance (A) can also be equated to emittance (E) under the assumption of thermal equilibrium and gray body behavior in the studied spectral range, according to Kirchhoff's law of thermal radiation [16, 18]. Therefore, equations 1 to 6 were used to theoretically calculate the T, R, and E of the fabrics under normal incidence of infrared laser radiation ($\lambda = 8\text{-}14 \mu\text{m}$).

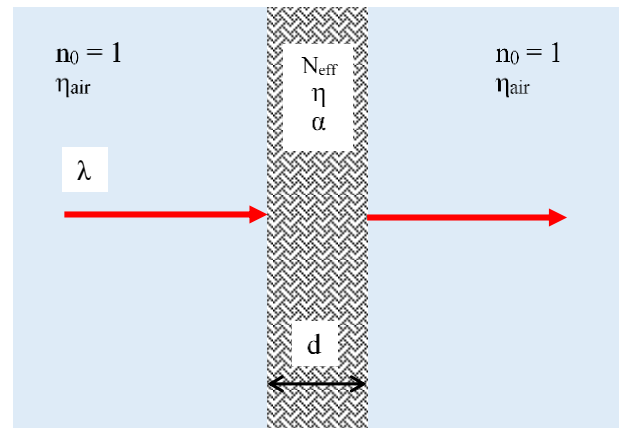


Fig. 1 Schematic of the fabric exposed to the IR laser beam of the FTIR spectrometer. n_0 , refractive index of air ($n_0 \approx 1$); η_{air} , intrinsic impedance of air (numerically equal to η_0 , the intrinsic impedance of free space).

Table 1 Properties of the fabric samples

Sample	Weft's linear density (den)	Weft per centimeter	Weight per unit area (g/m^2)	Thickness (μm)	Cloth cover factor
PP	80.0	56	127.83	319	0.95
PA1	74.2	59	129.62	305	0.96
PA2	61.3	60	125.99	311	0.93
PET	110	55	113.49	270	0.81

In summary, the derivation of the optical parameters follows a sequential logical flow: First, the attenuation coefficient (α) was calculated from the measured transmittance spectrum using Equation (1). Second, the effective refractive index (N_{eff}) was obtained from ATR measurements. Subsequently, the intrinsic impedance (η) was derived from N_{eff} using Equation (2). These parameters were then used to populate the ABCD transmission matrix (Equation 3), which models the fabric as a planar electromagnetic medium. Finally, the scattering parameters (S_{11} and S_{21}) were calculated from the ABCD matrix (Equation 4) to determine the reflectance (R) and transmittance (T) at normal incidence. Energy conservation (Equation 5) was then applied to calculate emittance (E).

2-3 Thermal properties of the fabrics

The effective reduction of the infrared transmission through the textiles was assessed using an IR thermometer (Fluke 62 Mini, USA) and by calculating the apparent temperature difference (Equation 6). Measurements were taken at outdoor temperature (0°C) and indoor temperature (21°C).

$$\Delta T_{\text{app}} = T_b - T_a \quad (6)$$

Where T_b is the temperature of the human skin, taken as 33 °C for this study. T_a is the apparent temperature on the fabric surface, ΔT_{app} (differences in apparent temperature) has the potential to help in determining the quantity of IR radiation obstructed by the fabric [19]. The physical significance of a higher apparent temperature difference (ΔT_{app}) is directly related to the fabric's radiative heating performance. A larger ΔT_{app} indicates a greater reduction in radiative heat loss from the skin to the environment. This occurs because fabrics with high infrared reflectance effectively trap body radiation between the skin and the fabric interior, creating a localized warming effect. Consequently, the outer fabric surface temperature (T_a) measured by the IR thermometer decreases relative to the skin temperature (T_b), resulting in an increased ΔT_{app} . This metric therefore, serves as a practical indicator of a fabric's ability to provide passive radiative heating by quantifying its efficiency in suppressing radiative heat transfer [19].

3 RESULTS AND DISCUSSIONS

Fig. S1 shows the refractive index of the raw materials and fabric samples in the mid-infrared region (see Supporting Information). The fabric can be considered as a composite material including a polymer, Al particles, and air. The refractive index of the multicomponent materials is expressed by the effective refractive index (N_{eff}) [20-22]. In the IR range of 2.5 to 14.5 μm , the refractive index of Al changes from 3.18 to 42.23. In the same IR range, the refractive index of the PP and PET polymers was less than 3 (Fig. S1, Supporting information). As a result, the N_{eff} of the PA1 and PA2 fabrics

increased, as compared to the PP fabric, due to the presence of Al particles (Fig. S2). S_{21} and S_{11} were calculated by N_{eff} and the attenuation coefficient of the fabric samples. There was an acceptable agreement between the theoretical calculation ($|S_{21}|^2$) and the experimental measurement (FTIR) regarding the IR transmittance of the fabric samples (Fig. 2), thus showing that the theoretical method used could also be valid for calculating the IR reflectance of the fabrics. The strong agreement between experimental and theoretical data for the pure PP sample (Fig. 2a) is due to its homogeneous structure and minimal scattering effects. Unlike the Al-composite samples, PP's uniform nature allows the ABCD model to accurately predict its behavior, as the model idealizes the fabric as a homogeneous layer. The absence of scattering particles like aluminum simplifies the optical interaction, leading to excellent model fidelity [16, 23]. This confirms the model's robustness for homogeneous materials, while the slight deviations in PA1 and PA2 results are expected due to the complexity of modeling scattering in heterogeneous systems.

By calculating $|S_{11}|^2$, the reflectance at the angle of 0° could be predicted. Fig. 3a shows the calculated reflectance spectra of the fabrics. The reflectance value of the fabrics consisting of PP/Al fibers was significantly higher than that of the PP and PET fabrics (Table 2).

The more pronounced spectral features observed in the PA1 sample, compared to PA2, are attributed to wavelength-dependent Mie scattering and interference effects from the dispersed Al particles. The higher Al content in PA2 likely leads to stronger particle-particle interactions and agglomeration, which can broaden and suppress resonant spectral features [24].

The transmittance spectrum for the specimens was calculated and depicted in Fig. 3b. The difference in the results between the PP and PET fabrics could be attributed to their chemical nature. The Al microparticles in the PA1 and PA2 samples resulted in more than a 60% reduction in the IR transmittance compared to the PP sample. The IR spectrum of Al within the studied range has no characteristic peaks and only has specular reflection. It appears that the presence of Al microparticles causes reflection and scattering, which reduces the thermal radiation transmission through the fabrics consisting of PP/Al yarns. This conclusion is further supported by Fig. 3a, where the average specular reflectance for the PP, PET, PA1, and PA2 samples is 2.57%, 11.15%, 43.52%, and 46.44%, respectively. The emittance of the fabrics decreased due to the presence of Al particles (Fig. 1c). The room temperature emissivity of Al is about 0.02, which prevents thermal radiation loss [25]. It should be noted that the reflection from the uneven surface of textiles included specular and diffuse reflection. In this research, the calculated $R(0^\circ)$ is a parameter considered for evaluating the reflectivity of the fabric samples.

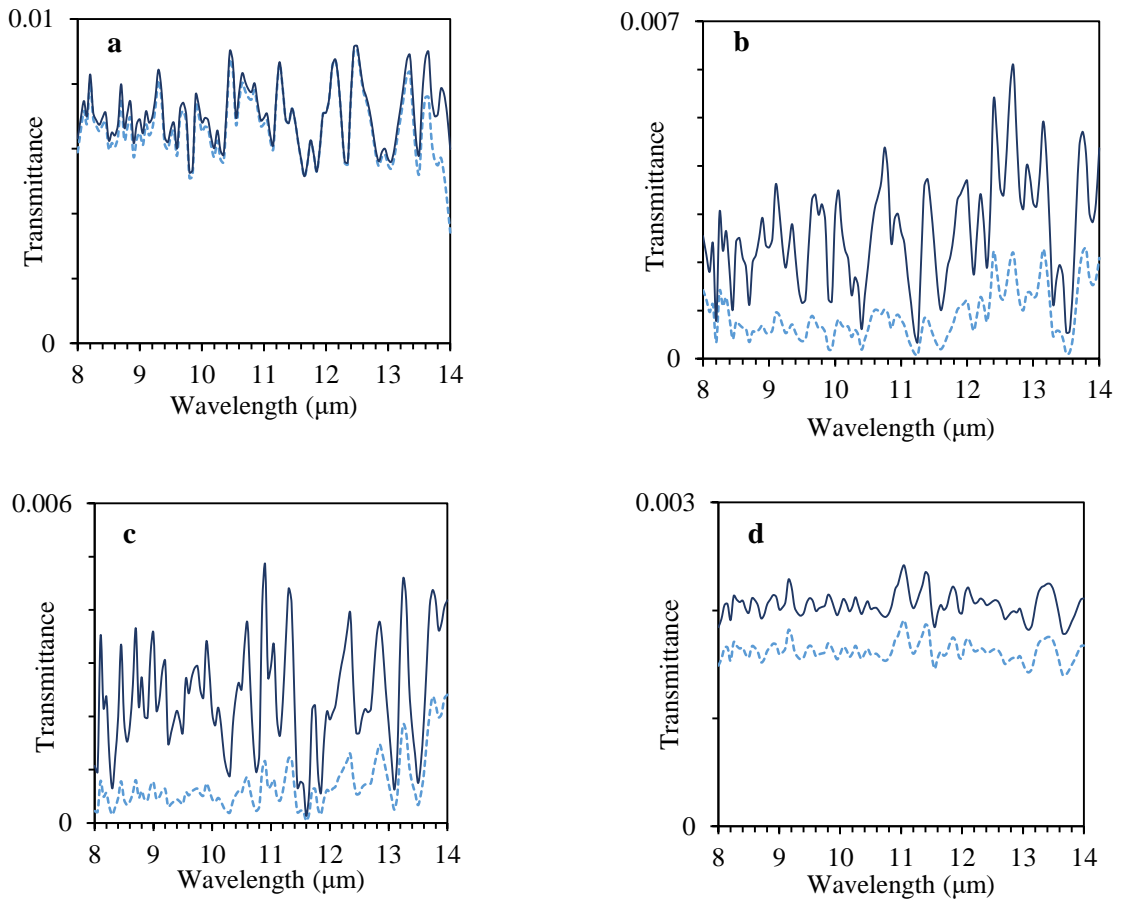


Fig. 2 The IR transmittance of the fabric samples based on theoretical calculation ([S21]2; dashed line) and experimental measurement (FTIR; solid line) for (a) PP, (b) PA1, (c) PA2, and (d) PET specimens

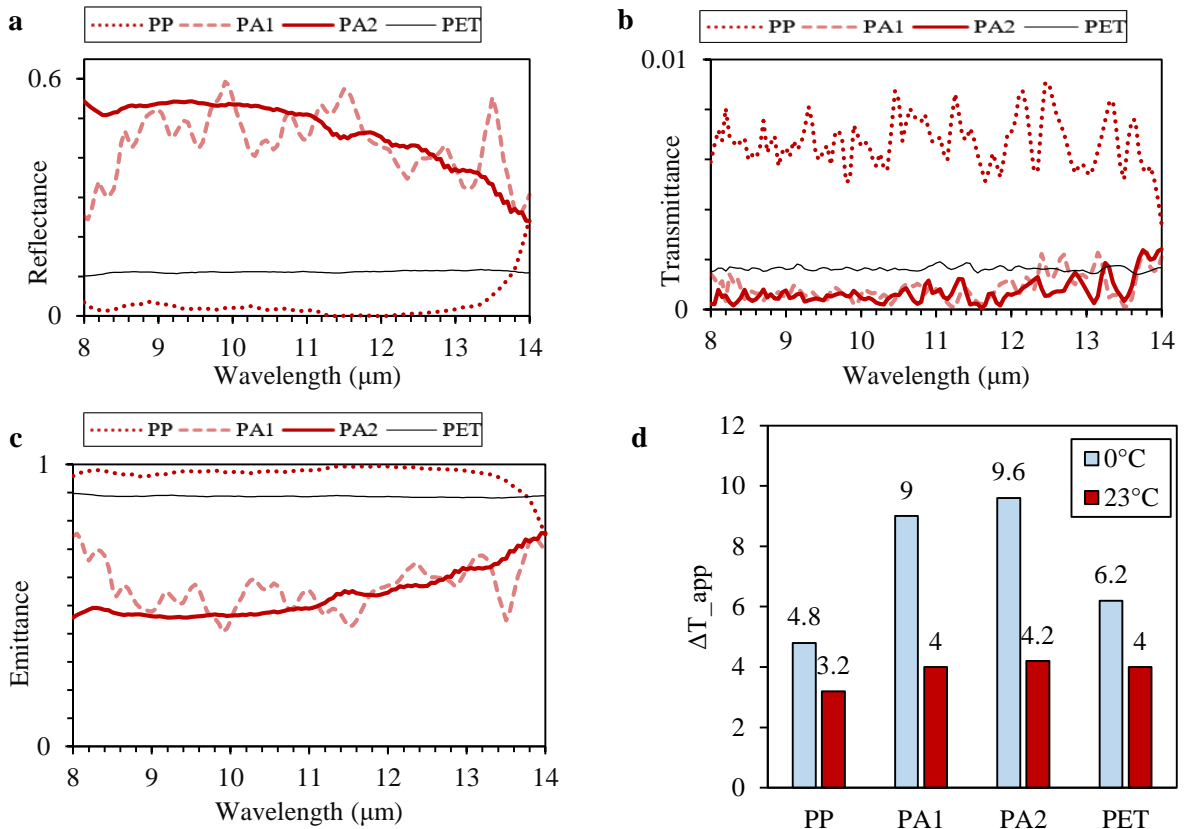


Fig. 3 (a) The reflectance, (b) transmittance, and (c) emittance spectra were calculated for the fabric samples in the range of human body thermal radiation (8-14 μm). (d) Differences in apparent temperature induced by the fabric samples at 0 and 23 $^{\circ}\text{C}$. A larger ΔT_{app} indicates stronger radiative heat trapping by the fabric layer

Fig. 3 and Table 2 confirm that the fabrics containing Al particles exhibit high reflectance, low transmittance, and low emittance. Consequently, these samples can provide thermal heating functionality by preventing the loss of body heat radiation [2, 11]. As shown in Fig. 3d, the apparent temperature difference created by the PA1 and PA2 samples (especially in cold environments) is higher than that of the control sample (PP) and conventional woven fabric (PET). Since ΔT_{app} represents the amount of heat radiation suppressed by the fabric, a larger ΔT_{app} implies stronger radiative heating performance. The trapped radiation between the human skin and the fabric can result in an elevation of skin temperature and provide thermal comfort in cold weather [26].

Table 2 The average of reflectance, transmittance, and emittance (%) was calculated for the fabrics at normal incidence (0°) in the range of human body radiation (8-14 μm)

Sample	Reflectance	Transmittance	Emittance
PET	11.15	0.16	88.69
PP	2.57	0.67	96.76
PA1	43.52	0.09	56.39
PA2	46.44	0.07	53.49

4 CONCLUSIONS

This study developed and validated a novel method for predicting the normal-incidence optical properties (R, T, E) of textiles in the infrared region by combining FTIR/ATR data with ABCD matrix calculations. This approach provides a viable and accessible alternative to integrated sphere measurements. Applying this method, we systematically evaluated woven fabrics and demonstrated that those incorporating aluminum particles (PA1: 1% Al, PA2: 2% Al) exhibited superior thermal radiation management compared to control samples (PP and PET). Key findings include:

- **Reflectance:** The PA1 and PA2 fabrics achieved average reflectance values of 43.52% and 46.44%, respectively, at 0° incidences, which were significantly higher than those of PP (2.57%) and PET (11.15%). These results demonstrate their ability to reflect body heat radiation effectively.
- **Transmittance:** The inclusion of Al particles reduced the IR transmittance by over 60%, with PA1 and PA2 transmitting only 0.09% and 0.07% of the radiation, respectively, compared to PP (0.67%).
- **Emittance:** The emittance values decreased to 56.39% (PA1) and 53.48% (PA2), attributable to Al's low intrinsic emissivity (~ 0.02), thereby minimizing the radiative heat loss.
- **Thermal Performance:** Apparent temperature differences (ΔT_{app}) measured at 0°C and 21°C underscored the heating capability of Al-containing fabrics, with PA1 and PA2 showing the highest ΔT_{app} due to trapped radiation between the fabric and skin.

To isolate the effect of Al particles, all samples were standardized in warp yarn composition and weave structure (twill 3/1). The variations in weft density (PA1: 59 wefts/cm, PA2: 60 wefts/cm) and other structural parameters were an inherent result of the altered physical properties of the PP/Al yarns, as detailed in Section 2.1. Consequently, the consistent trends in enhanced reflectance and reduced transmittance/emittance with increasing Al content demonstrate that the observed improvements in thermal radiation management stem primarily from the Al modification.

The proposed method (calculating the optical parameters (α , N_{eff}) from the FTIR/ATR data and deriving R, T, and E via ABCD matrices) showed strong agreement with the experimental measurements. For instance, the correlation between the theoretical calculation ($|S_{21}|^2$) and the experimentally measured FTIR transmittance yielded a coefficient of determination of $R^2 > 0.95$. The proposed method in this research provides a viable and accessible tool for the relative evaluation and comparison of the thermal radiation properties of textiles, particularly in situations where advanced equipment such as integrating spheres is not available.

These results highlight the potential of Al-modified fabrics as passive radiative heating textiles, combining theoretical rigor with practical thermal comfort solutions for cold environments.

4-1 Limitations and Scope for Generalization

While the proposed method provides a viable and accessible tool for evaluating textile radiation properties, its applicability is subject to certain constraints inherent to the model's assumptions and the physical parameters of the fabrics.

- **Model Assumptions and Applicability:** The core of our approach relies on modeling the fabric as a homogeneous, planar layer with effective optical properties (α and N_{eff}). This assumption holds well for the studied woven samples with relatively consistent thickness and surface topography. However, the model's accuracy may diminish for fabrics with extreme surface roughness, high porosity, significant transparency, or pronounced heterogeneity that deviates substantially from a planar layered structure. For instance, highly open knits or nonwovens with complex 3D fiber arrangements might introduce scattering effects.
- **Furthermore,** the optical properties (R, T, E) calculated in this study are for normal incidence ($\theta_i = 0^\circ$). While this provides a valuable benchmark for comparing the intrinsic radiative performance of textiles, human body radiation is hemispherical. For a comprehensive prediction of thermal comfort in real-world wearing conditions, future work should integrate these fundamental properties with models that account for angular dependence and the microclimate (temperature and humidity) between the skin and the fabric.
- **Influence of Physical Parameters:** The model directly incorporates fabric thickness (d) as a critical input. While this study used a standardized thickness for optical measurements, variations in thickness across a fabric roll or between production batches would directly impact the

calculated attenuation (α) and, consequently, the predicted T, R, and E. Therefore, for accurate comparisons, thickness must be carefully controlled or measured at the exact location of optical testing. Furthermore, parameters like porosity and yarn density are indirectly accounted for in the measured values of α and N_{eff} . The model does not explicitly disentangle their individual contributions, meaning that two fabrics with different structures but similar effective optical parameters would be calculated to have similar radiative properties.

- Scope for Generalization: The methodology is most robust for the relative comparison of textiles with similar structural characteristics (e.g., weave type, weight, and thickness). Generalization to a vastly broader range of textile architectures requires further validation against standard methods for each new category of material (e.g., knits, felts, coated fabrics) to define the boundaries of the model's validity.

REFERENCES

- [1] Zhang, Y., Li, Y., Li, K., Kwon, Y.S., Tennakoon, T., Wang, C., et al., 2022. A large-area versatile textile for radiative warming and biomechanical energy harvesting. *Nano Energy*, 95, p.106996.
- [2] Peng, Y. and Cui, Y., 2020. Advanced textiles for personal thermal management and energy. *Joule*, 4(4), pp.724-742.
- [3] Hu, R., Liu, Y., Shin, S., Huang, S., Ren, X., Shu, W., et al., 2020. Emerging materials and strategies for personal thermal management. *Advanced Energy Materials*, 10(17), p.1903921.
- [4] Tong, J.K., Huang, X., Boriskina, S.V., Loomis, J., Xu, Y. and Chen, G., 2015. Infrared-transparent visible-opaque fabrics for wearable personal thermal management. *ACS Photonics*, 2(6), pp.769-778.
- [5] Yue, X., Zhang, T., Yang, D., Qiu, F., Wei, G. and Zhou, H., 2019. Multifunctional Janus fibrous hybrid membranes with sandwich structure for on-demand personal thermal management. *Nano Energy*, 63, p.103808.
- [6] Ke, Y., Wang, F., Xu, P. and Yang, B., 2018. On the use of a novel nanoporous polyethylene (nanoPE) passive cooling material for personal thermal comfort management under uniform indoor environments. *Building and Environment*, 145, pp.85-95.
- [7] Hsu, P.-C., Liu, X., Liu, C., Xie, X., Lee, H.R., Welch, A.J., et al., 2014. Personal thermal management by metallic nanowire-coated textile. *Nano letters*, 15(1), pp.365-371.
- [8] Cai, L., Song, A.Y., Li, W., Hsu, P.C., Lin, D., Catrysse, P.B., et al., 2018. Spectrally Selective Nanocomposite Textile for Outdoor Personal Cooling. *Advanced Materials*, 30(35), p.1802152.
- [9] Jafar-Zanjani, S., Salary, M.M. and Mosallaei, H., 2017. Metafabrics for thermoregulation and energy-harvesting applications. *ACS Photonics*, 4(4), pp.915-927.
- [10] Zandavi, S.H., Huang, Y., Ni, G., Pang, R., Osgood III, R.M., Kamal, P., et al., 2017. Polymer Metamaterial Fabrics for Personal Radiative Thermal Management. In: *Proceedings of the Frontiers in Optics Conference*, p.FM4D.6.
- [11] Cai, L., Song, A.Y., Wu, P., Hsu, P.-C., Peng, Y., Chen, J., et al., 2017. Warming up human body by nanoporous metallized polyethylene textile. *Nature communications*, 8(1), p.496.
- [12] Tavakkol, E., Borhani, S., Nezhad, A.Z., Shanbeh, M. and Alsharif, M.A., 2023. Fabrication and Characterization of Polypropylene/Aluminum Fibers for Wearable Applications in the Infrared Region. *Fibers and Polymers*, 24(3), pp.987-1001.
- [13] Tavakkol, E., Borhani, S., Nezhad, A.Z., Shanbeh, M. and Alsharif, M.A., 2023. Passive radiative personal heating by woven fabrics containing aluminum particles. *Materials Today Energy*, 31, p.101226.
- [14] Chen, H., Baitenov, A., Li, Y., Vasileva, E., Popov, S., Sychugov, I., et al., 2019. Thickness Dependence of Optical Transmittance of Transparent Wood: Chemical Modification Effects. *ACS Applied Materials & Interfaces*, 11(38), pp.35451-35457.
- [15] Sayed, F.A., Elsayed, H.A. and Aly, A.H., 2020. Optical properties of photonic crystals based on graphene nanocomposite within visible and IR wavelengths. *Optical and Quantum Electronics*, 52(10), pp.1-16.
- [16] Sun, J. and Lucyszyn, S., 2018. Extracting complex dielectric properties from reflection-transmission mode spectroscopy. *IEEE Access*, 6, pp.8302-8321.
- [17] Pozar, D.M., 2011. *Microwave Engineering*, 4th ed. Hoboken, NJ: John Wiley & Sons.
- [18] Howell, J.R., Mengüç, M.P., Daun, K. and Siegel, R., 2020. *Thermal Radiation Heat Transfer*. Boca Raton, FL: CRC Press.
- [19] Rubežienė, V., Padleckienė, I., Žuravliova, S.V. and Baltušnikaitė, J., 2013. Reduction of thermal signature using fabrics with conductive additives. *Materials Science*, 19(4), pp.409-414.
- [20] Altunin, K.K. and Gadomsky, O.N., 2012. High-negative effective refractive index of silver nanoparticles system in nanocomposite films. *Optics Communications*, 285(5), pp.816-820.
- [21] Jia, Z., 2005. Determination of the effective refractive index of porous silicon/polymer composite films. *Chinese Optics Letters*, 3(10), pp.608-610.
- [22] Liu, S., Islam, M.D., Ku, Z., Boyd, D.A., Zhong, Y., Urbas, A.M., et al., 2021. Novel computational design of high refractive index nanocomposites and effective refractive index tuning based on nanoparticle morphology effect. *Composites Part B: Engineering*, 223, p.109128.
- [23] Bohren, C.F. and Huffman, D.R., 2008. *Absorption and Scattering of Light by Small Particles*. Hoboken, NJ: John Wiley & Sons.

- [24] Balanis, C.A., 2012. Advanced Engineering Electromagnetics. Hoboken, NJ: John Wiley & Sons.
- [25] De Silva, H.T., 2014. Development of Thermal Insulating Textiles. Ph.D. Dissertation, Hochschule Niederrhein, Mönchengladbach, Germany.
- [26] Yue, X., He, M., Zhang, T., Yang, D. and Qiu, F., 2020. Laminated Fibrous Membrane Inspired by Polar Bear Pelt for Outdoor Personal Radiation Management. ACS Applied Materials & Interfaces, 12(10), pp.12285-12293.